Computers and Geotechnics 80 (2016) 138–151

Contents lists available at ScienceDirect

Computers and Geotechnics

journal homepage: www.elsevier.com/locate/compgeo

Research Paper

Three-dimensional effects of a deep excavation on wall deflections in loose to medium dense sands

Bin-Chen Benson Hsiung [a,*], Kuo-Hsin Yang [b], Wahyuning Aila [b], Ching Hung [c]

[a] Department of Civil Engineering, National Kaohsiung University of Applied Sciences, 415, Chen Kung Road, Kaohsiung 807, Taiwan
[b] Department of Civil and Construction Engineering, National Taiwan University of Science and Technology (Taiwan Tech), 43, Sec. 4, Keelung Rd., Taipei 106, Taiwan
[c] Department of Civil Engineering, National Cheng Kung University, 1, University Rd., Tainan 701, Taiwan

ARTICLE INFO

Article history:
Received 17 February 2016
Received in revised form 30 June 2016
Accepted 3 July 2016

Keywords:
Deep excavation
Loose to medium dense sand
Wall deflection
Three-dimensional effect
Plane strain ratio (PSR)

ABSTRACT

This paper presents a study that evaluates the three-dimensional effects of a deep excavation on wall displacements in loose to medium dense sands. A finite element (FE) analysis is then conducted to verify the performance of 3D FE models in predicting wall displacements and results indicate that the use of the Mohr-Coulomb model with the soil modulus obtained from in-situ dilatometers for loose to medium dense sands yields reasonable predictions of the excavation-induced wall displacements. Based on the parametric study, the plane strain ratio (PSR), was determined for excavations in loose to medium dense sand.

1. Introduction

The magnitude and shape of wall displacements that are induced by a deep excavation depend on numerous factors, such as the soil and groundwater conditions, excavation geometry, surcharge load, existence of adjacent structures, construction method, stiffness and penetration of the retaining wall, type and installation method of the struts, spacing and stiffness of the struts, and ground improvement. Furthermore, in certain excavations, the magnitude and shape of the wall displacement are also affected by the distance from the evaluated section to the corner of the excavation. The effect of the section's position on the displacement is known as the three-dimensional effect or the corner effect.

Many studies have investigated the behaviour of wall affected by deep excavations, including Clough and O'Rourke [1], Ou et al. [2,3], Ou [4], Kung et al. [5], Lin et al. [6], Hsiung [7], Schweiger [8], Wang et al. [9], Likitlersuang et al. [10], Khoiri and Ou [11], Finno et al. [12], Orazalin et al. [13] and Hsieh et al. [14]. Most of these studies have addressed excavations in clays, and few have reported excavations in sand. Nikolinakou et al. [15] conducted a feedback analysis using the MIT S1 soil model to analyse excavations in sand in Berlin, Germany. The retaining and strutting systems and soil properties of the excavation that was examined by [15] are different from the excavation case in this study.

The concept of the plane strain ratio (PSR), which was first proposed by Ou et al. [2], is the ratio of the maximum wall deflection of a section of a wall to the maximum wall deflection of the section under plane strain conditions. The PSR values were determined and evaluated for a typical excavation in clayey soils in Taipei, Taiwan. The concept of the PSR is adopted in this study to quantify the 3D effects of an excavation in sand on the wall deformation. The influence of the soil type (sand and clay) is also examined by comparing the PSR chart proposed by Ou et al. [2] for excavations in clay with the chart developed in this study for excavations in sand.

This paper presents a *unique* case of detailed, well-documented, and reliable observations of a 16.8-m-deep excavation in sand. The excavation is nearly completely embedded in thick layers of loose (SPT-N values, N ⟨1 0) to medium dense (N = 10–30) sands. Detailed background information about the subsurface soil conditions, in-situ and laboratory soil tests, construction sequences and monitoring data are first introduced and discussed. The input soil parameters were determined using test results from both in-situ dilatometer tests (DMTs) and laboratory tests (triaxial and direct shear tests). Moreover, the determined soil parameters were also compared with the values predicted by several empirical approaches (correlations with SPT and CPT) to confirm the reliability of the parameters that were used in the analyses. A finite

* Corresponding author.
E-mail addresses: benson.hsiung@gmail.com (B.-C.B Hsiung), khy@mail.ntust.edu.tw (K.-H. Yang), wahyuningaila@gmail.com (W. Aila), chinghung@mail.ncku.edu.tw (C. Hung).

http://dx.doi.org/10.1016/j.compgeo.2016.07.001
0266-352X/

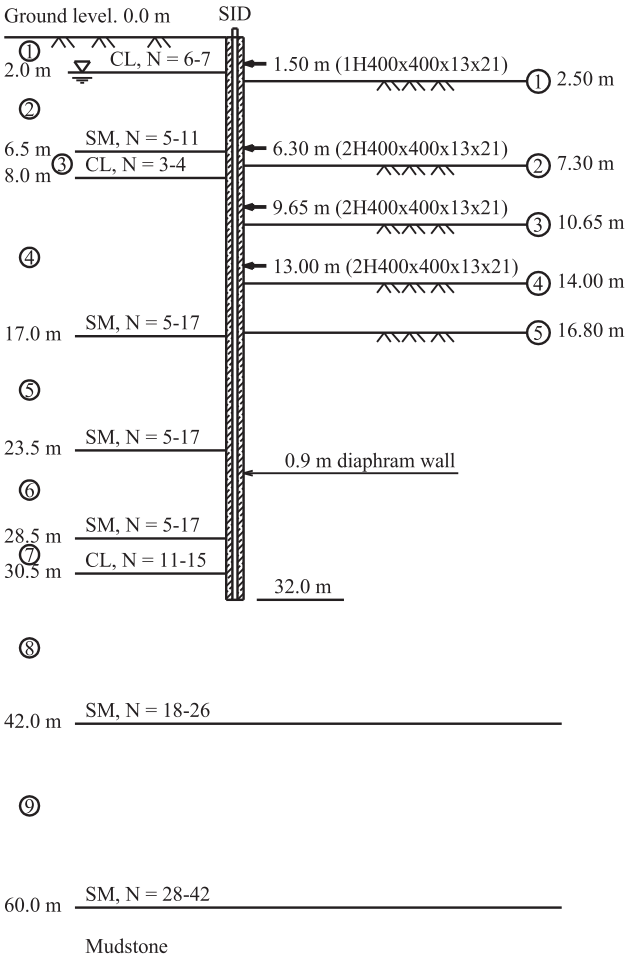

Fig. 1. Cross section and soil profile of the excavation.

element (FE) analysis was then conducted to model the selected deep excavation in Kaohsiung, Taiwan, to verify the performance of 3D FE models in predicting wall displacements. The results of the numerical analysis and field observations are compared and discussed. Finally, a PSR chart for excavations in sand is developed using a series of parametric studies with several excavation aspect ratios. The proposed PSR chart can facilitate practical designs (typically in 2D) to account for the 3D effects of excavations on wall deformation.

2. Project background

2.1. Description of excavation site condition

A deep excavation in the central part of Kaohsiung city, Taiwan, is selected for case study and numerical simulation. The excavation was 70 m long and 20 m wide. The construction was carried out using the bottom-up method in 5 excavation stages with 4-level steel struts, and the maximum excavation depth was 16.8 m in the final excavation stage. The excavated pit was retained by a 0.9-m-thick and 32-m-deep diaphragm wall. Fig. 1 shows the cross section and subsurface soil profile of the excavation, and Fig. 2 shows an overview of the excavation and strutting system. Table 1 summarizes the details of the construction sequence of the project.

As shown in Fig. 1, highly permeable, loose-to-medium dense sand is observed from the ground surface to a depth of approximately 42 m, and two layers of clay are occasionally present (depths of 6.5 m to 8.0 m and 28.5 m to 30.5 m below the surface). Based on the United Soil Classification System, the sand and clay are classified as silty sand (SM) and low plasticity clay (CL). The SPT-N (N) values of the sand from 2.0 to 6.5 m below the surface range from 5 to 11, and those for the sand from 8.0 to 28.5 m range from 5 to 17. The sand deeper than 30.5 m below the surface is much denser (N values between 18 and 26), and the sand from 42.0 m to 60.0 m below the surface has N values from approximately 28–42.

The permeability of the lower clay (28.5–30.0 m below the surface) tends to be extremely low and thus limits the flow of water into the base of the excavation, although pumping inside the excavation had to be carried out during the construction. The initial groundwater level was observed at 2 m below the surface and did not change considerably until the end of the excavation. In

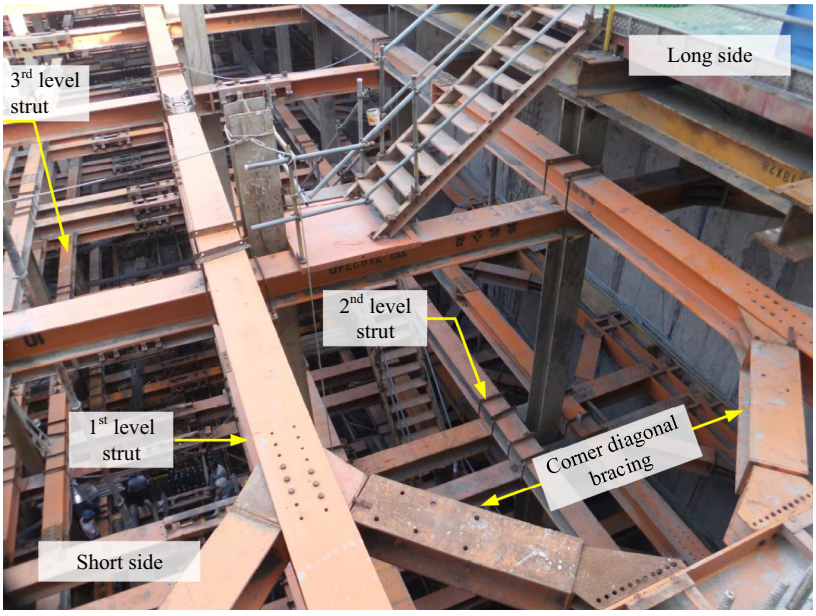

Fig. 2. Overview of the excavation and strutting system.

Table 1
Construction activities and sequence of the excavation in this study.

Construction sequence	Construction period	
	Start	End
Diaphragm wall installation	2012/09/19	2012/09/23
Kingpost installation	2012/09/24	2012/10/02
Phase 1		
Dewatering	2012/10/03	
Excavation to 2.5 m below the surface	2012/10/12	2012/10/17
1st level strut installation at 1.5 m below the surface	2012/10/17	2012/10/21
Phase 2		
Dewatering	2012/10/15	
Excavation to 7.3 m below the surface	2012/10/22	2012/10/25
2nd level strut installation at 6.3 m below the surface	2012/10/26	2012/10/30
Phase 3		
Dewatering	2012/10/27	
Excavation to 10.65 m below the surface	2012/10/31	2012/11/03
3rd level strut installation at 9.65 m below the surface	2012/11/04	2012/11/07
Phase 4		
Dewatering	2012/11/07	
Excavation to 14.0 m below the surface	2012/11/08	2012/11/11
4th level strut installation at 13.0 m below the surface	2012/11/11	2012/11/14
Phase 5		
Dewatering	2012/11/11	
Excavation to 16.8 m below the surface	2012/11/15	2012/11/19
Casting of floor base slab	2012/11/30	2012/12/03
Completion of the 1st slab at floor B4	2012/12/04	2012/12/12
Completion of the 2nd slab at floor B3	2012/12/13	2013/01/02
Completion of the 3rd slab at floor B2	2013/01/03	2013/01/19
Completion of the 4th slab at floor B1	2013/01/20	2013/02/05
Completion of the final slab at the ground floor	2013/02/06	2013/03/09

contrast, the groundwater level remained from 0 m to 8 m below the excavation level during the construction stage.

2.2. In-situ monitoring and observations

The observations of the excavation are discussed in this section. The instruments that were used to monitor the behaviour of the ground and structure due to the deep excavation include inclinometers in both the diaphragm wall (SID) and soils (SIS), settlement markers on the ground and buildings, building tiltmeters, observation wells inside and outside the excavation, and vibration wire gauges (VG) on the strut. Fig. 3 shows the overall layout of the instruments installed at the site.

The observations of lateral wall displacement are examined first. The wall behaved first in cantilever-mode and then changed to prop-mode after the struts were installed. The corner effect is likely the reason for the wide variation in the maximum wall displacement because the displacement measured by the

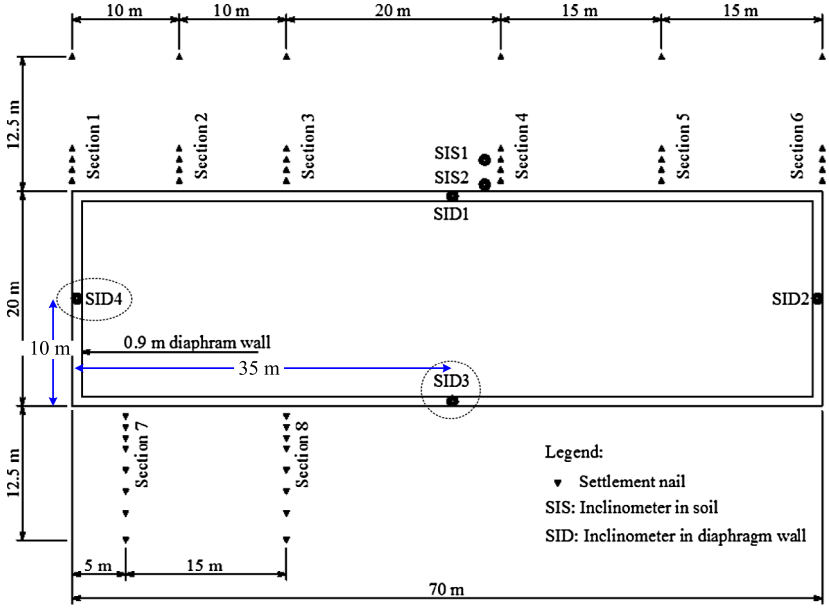

Fig. 3. Layout of instruments installed at the site.

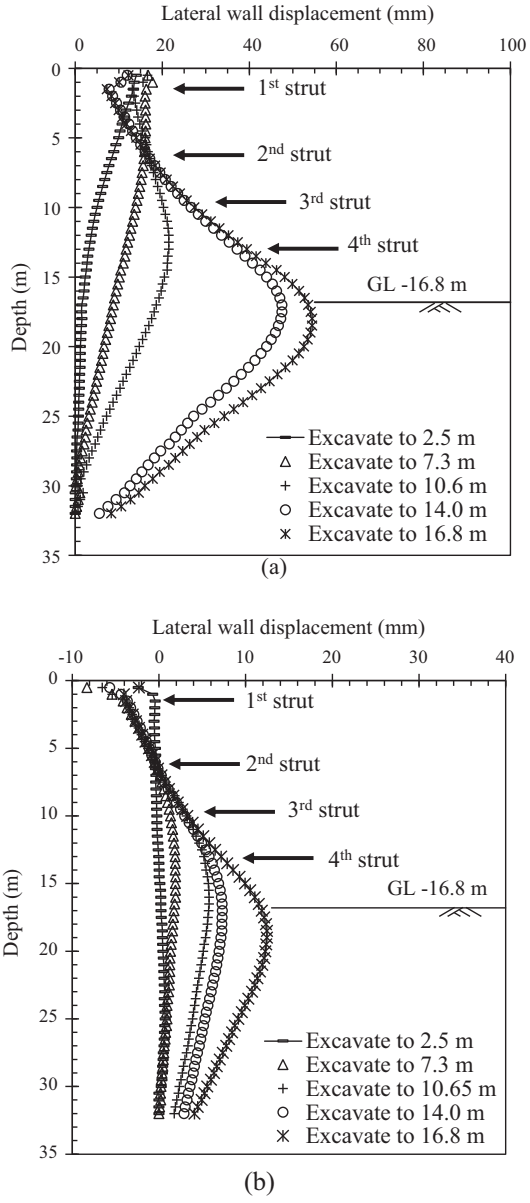

Fig. 4. Monitored wall displacements: (a) SID3; (b) SID4.

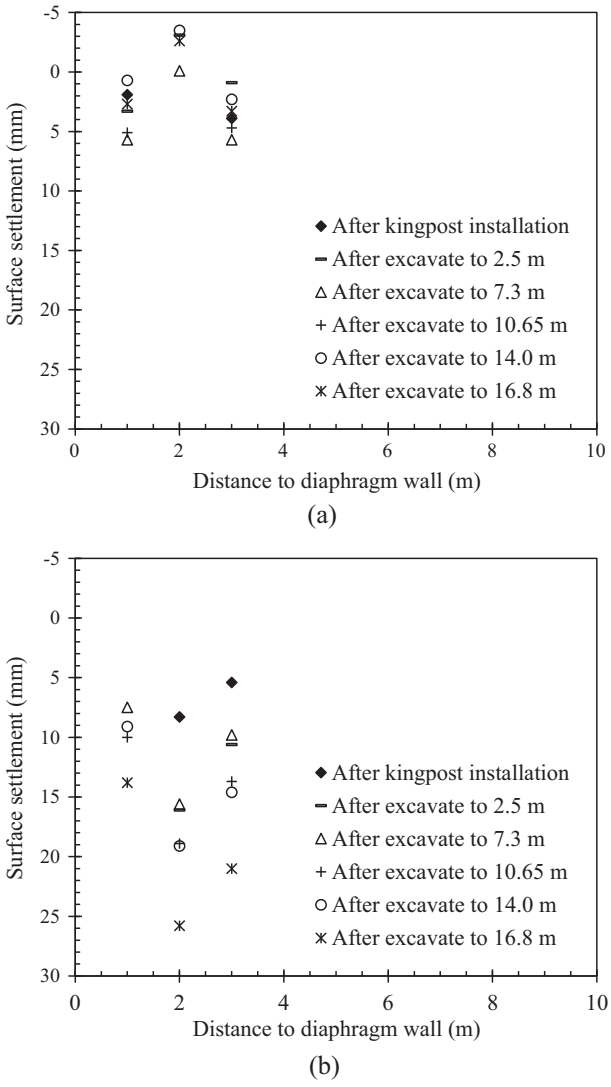

Fig. 5. Selected surface settlement measurements: (a) Section 1 (at the corner of the wall); (b) Section 4 (at the centre of the long wall).

inclinometer located on the short side is considerably smaller than that measured by the inclinometer on the long side (Fig. 4). In this case, the maximum wall displacements on the short side and long side gradually increased as the excavation progressed to 8.6 mm and 54.4 mm, respectively, at the end of excavation.

Eight monitoring sections were installed to measure the ground settlements outside the perimeter of the excavation. However, because the site is next to a main road with heavy traffic, reliable measurements can only be taken up to 3 m from the diaphragm wall. Fig. 5 shows the ground surface settlement measured from Sections 1 and 4. A shown in Fig. 3, Section 1 is located at the corner of the wall, and Section 4 is located at the centre of the long side wall. The measurements indicate that the maximum surface settlement reaches approximately 25 mm at the end of the excavation, whereas the maximum surface settlement gradually decreases as the measured section approaches the corner.

The strut loads were monitored continuously during the different excavation stages (Fig. 6). The maximum strut load was approximately 1500 kN from the 2nd to 4th level struts at the end of the excavation. However, the maximum strut load of the 1st level strut at the end of the excavation (Fig. 7) is considerably lower, which is likely because of the influence of the wall deformation pattern as excavation progressed (i.e., small wall deformation at the top). Fig. 7 compares the distributed prop load (DPL) diagrams that were proposed by Twine and Roscoe [16] and calculated from the measured strut loads in this study to the apparent earth pressure diagrams for excavations in sand that were proposed by Peck [17]. Based on a database of the strut loads from eleven case histories of excavations in granular materials from the UK, the USA, Germany, Brazil and Japan, Twine and Roscoe [16] proposed that the DPL in sand can be calculated as:

$$p = 0.2 \cdot \gamma \cdot H \tag{1}$$

where p is the distributed prop load (kN/m), γ is the unit weight of the granular soil, and H is the excavation depth. Notably, unlike the excavation case in this study, none of the case histories compiled by Twine and Roscoe [16] was an excavation completely in loose to medium dense sand.

Peck [17] proposed apparent earth pressure envelopes after making observations of several braced cuts. Peck's equation for sand is expressed as:

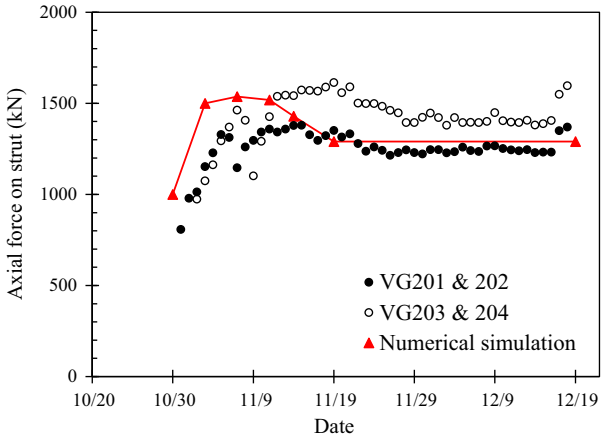

Fig. 6. Measured and predicted strut loads at the 2nd level strut (VG denotes vibration gauges for strut load measurements).

$$p = 0.65K_a \cdot \gamma \cdot H \quad (2)$$

where K_a is the active earth pressure coefficient, γ is the unit weight of sand, and H is the excavation depth. In both Eqs. (1) and (2), the earth pressure and the water pressure below the groundwater table were calculated separately, and the unit weight of the soil should be taken as the submerged unit weight γ'.

A comparison of the results in Fig. 7 shows that the apparent earth pressure diagram for sand suggested by Peck [17] and the DPL diagram by Twine and Roscoe [16] match well for these subsurface soil conditions (i.e., sand with an average ϕ' of 33°). The empirical equations by Twine and Roscoe [16] and Peck [17] generally agree well with the DPL calculated in this study at depths of 3–9 m. However, the two empirical methods, which involve the increase of water pressure with depth in the calculation, overestimate the distributed strut load at depths greater than 9 m. Because this comparison is based on only one measured DPL, additional case histories for excavations in loose to medium dense sand should be compiled for further evaluation and comparison.

Fig. 8 shows the variation of the groundwater levels inside and outside the excavation area. Because the excavation has to be conducted in high permeability sand with a shallow groundwater table (i.e., 3 m below the surface), pumping inside the excavation is essential to keep the water table at least 1 m below the excavation level. Therefore, the groundwater table inside the excavation gradually decreased as the excavation progressed. As a result of the impermeable reinforced concrete diaphragm wall and the presence of an impermeable clay layer near the toe of the wall, the groundwater table outside the excavation area seems to not be affected by pumping the water inside the excavation. Finally, the impacts of the excavation on the adjacent buildings were inspected and considered insignificant because limited settlement and tilting of the buildings were detected at the end of the excavation.

3. Soil Tests and determination of soil properties

3.1. In-situ soil tests

Fig. 9 shows detailed information from 3 boreholes (BH1, BH5 & BH7) located on site or nearby, including the profiles of the SPT-*N* values, sand and fines contents and void ratios (related to soil density) with depth. The *N* values remain lower than 10 to depths of approximately 10 m below the surface and less than 30 until a depth of 40 m. In most of the borehole logs, the sand contents are very high (between 80% and 90%) to the final excavation level (i.e., 16.8 m below the ground surface). The void ratios are also

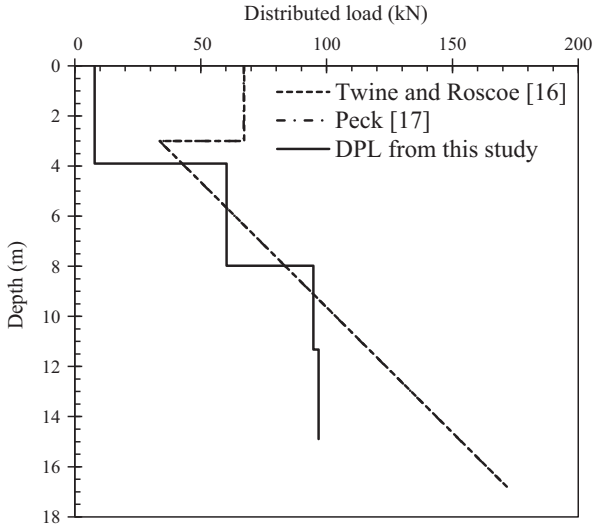

Fig. 7. Comparison of the distributed prop load (DPL) and apparent earth pressure diagrams for excavations in sand.

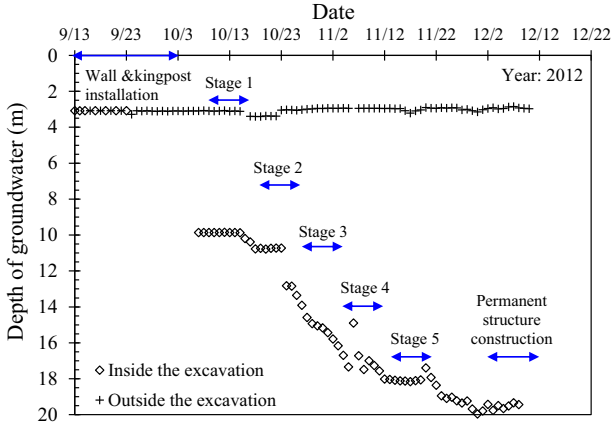

Fig. 8. Monitoring of groundwater levels inside and outside the excavation area during each construction stage (arrows indicate the construction period and excavation depth).

large (approximately 0.6 to 1.0), which indicates that the sand is loose to medium dense. The total unit weight of the soil ranges from 18.0 to 21.0 kN/m^3, and the water contents below the groundwater level range from 18% to 31%.

The SPT is a simple and useful in-situ test that is widely applied in various foundation design standards and codes worldwide, such as that of the Architectural Institute of Japan [18]. By collecting data from different soils, Stroud [19] developed empirical correlations of SPT-*N* values with soil shear strength and stiffness properties. Skempton [20] analysed data with SPT-*N*, effective vertical stress σ'_v and relative density information and demonstrated a linear relationship between *N* and σ'_v in sand. Fig. 10 shows a linear relationship between SPT-*N* and σ'_v for the excavation in sand in this study, which supports the observations of Skempton [20].

In addition to the SPT-*N* values and the soil physical properties that were evaluated, a series of DMTs and CPTs were conducted to further confirm the reliability of the soil strength and deformation parameters that were determined in this study. The maximum depths of the boreholes for the DMTs and CPTs were 30 m and 40 m, respectively. Fig. 11 shows the CPT readings, including the logs of the tip resistance q_c, side friction f_s and friction ratio F_r. At

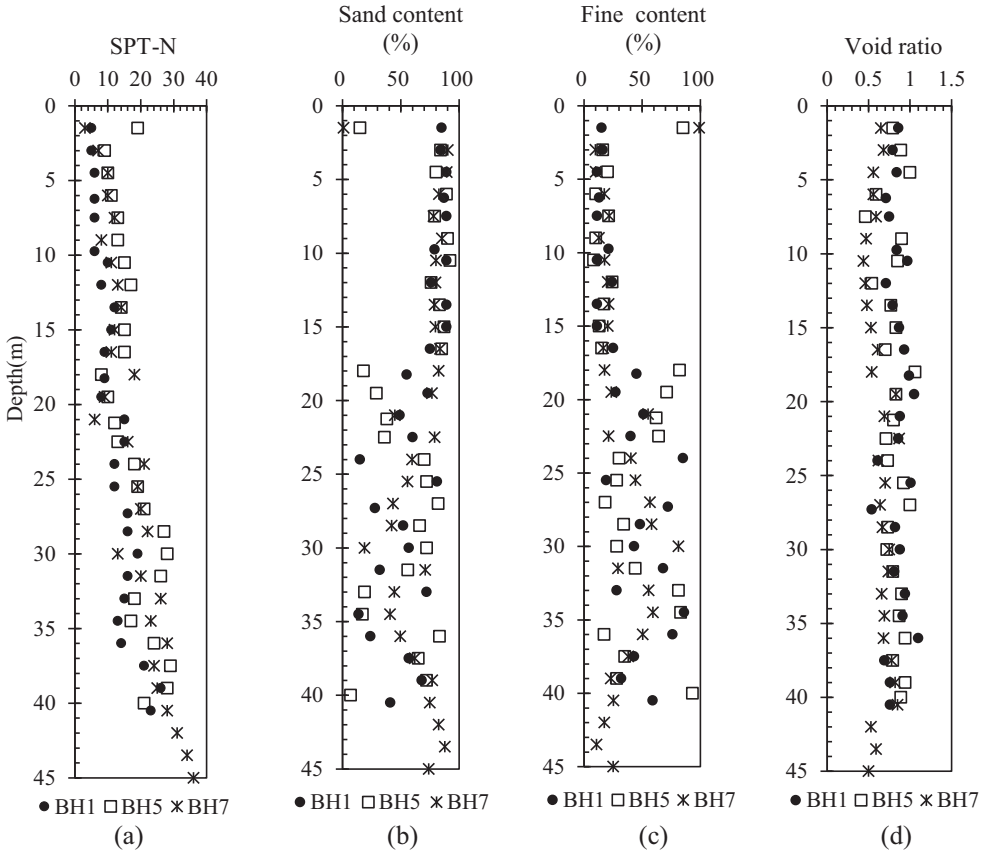

Fig. 9. Information from borehole logs: (a) SPT-N; (b) sand content; (c) fines content; and (d) void ratio.

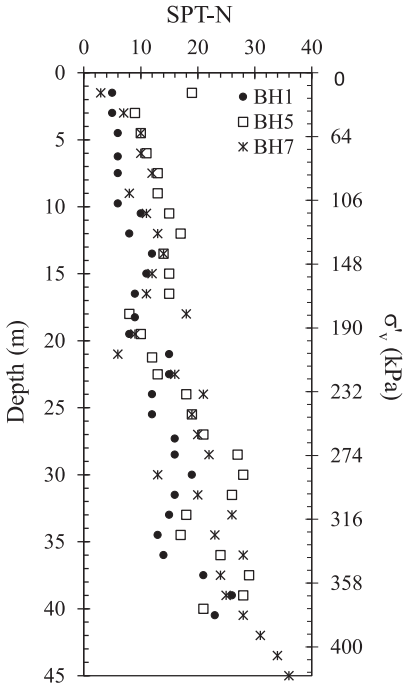

Fig. 10. Relationship between SPT-*N* value and σ'_v in sand.

the final excavation level, q_c reached 6000 kPa, and f_s reached approximately 45 kPa. The detailed test results of the DMTs and a comparison with the soil modulus estimated from the SPT and CPT correlations are discussed later.

3.2. Soil modulus and shear strength properties

Many previous studies have applied and assessed soil models for excavation modelling. Powire et al. [21] applied three soil constitutive models, namely the Mohr-Coulomb (MC) model, BRICK model, and Schofield model based on critical state soil mechanics, to simulate wall displacements induced by deep excavations in London clay and concluded that the wall movement predicted by the FE analyses depended more on the soil modulus than on the soil model. However, the calculated ground movement depends on both the soil model and the soil stiffness. Powire et al. [21] also found that all three soil models predicted ground heaves of up to 20 mm immediately behind the wall, and the MC model predicted a very large settlement (50 mm) at the far end of the excavation (approximately 50 m from the excavation). Jardine et al. [22] studied an excavation in London clay numerically using a non-linear soil model to accurately analyse the soil-structure interaction. Burland and Kalra [23] investigated the excavations for the Queen Elizabeth II Conference Centre in London Clay. Two types of soil moduli, undrained and drained, were considered for the analyses. Unlike the excavation in clay in Burland and Kalra [23], the excavation in this study is situated in very deep and thick loose sand, so the drained modulus, rather than the undrained modulus, is anticipated to play a key role.

In this study, the linearly elastic-perfect plastic MC model is adopted for the numerical simulation. The MC model has five parameters, including the friction angle ϕ, cohesion c, Young's modulus E, Poisson's ratio ν, and dilatation angle ψ. Because the soil modulus plays a key role in calculating the wall movement induced by an excavation, the soil moduli obtained from the in-situ and lab tests and estimated from empirical correlations are

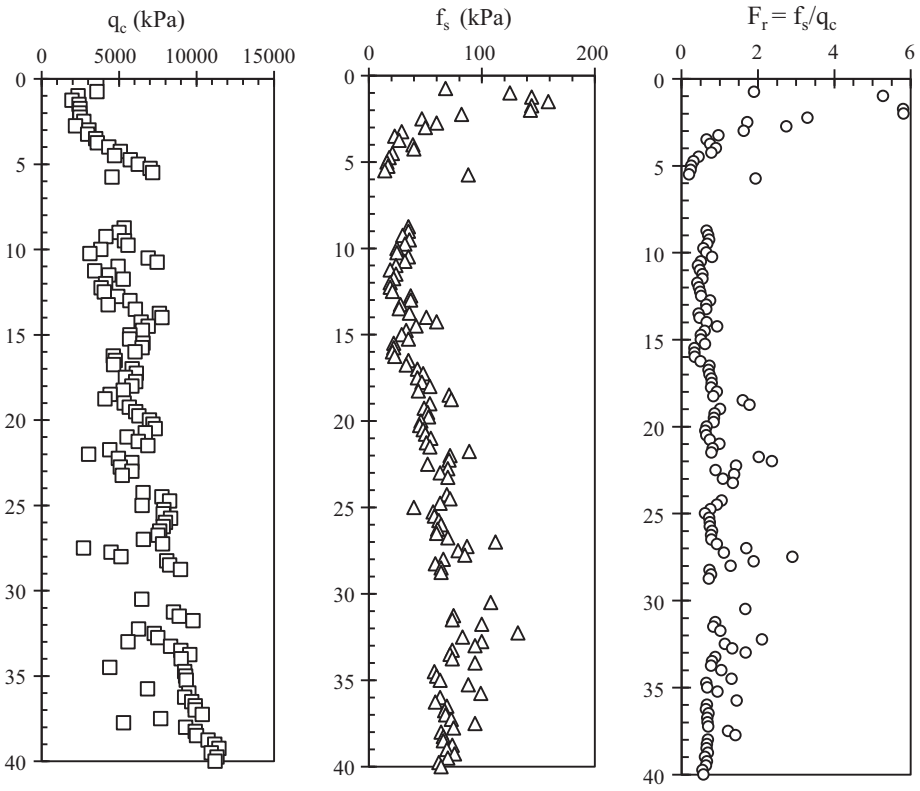

Fig. 11. CPT test results.

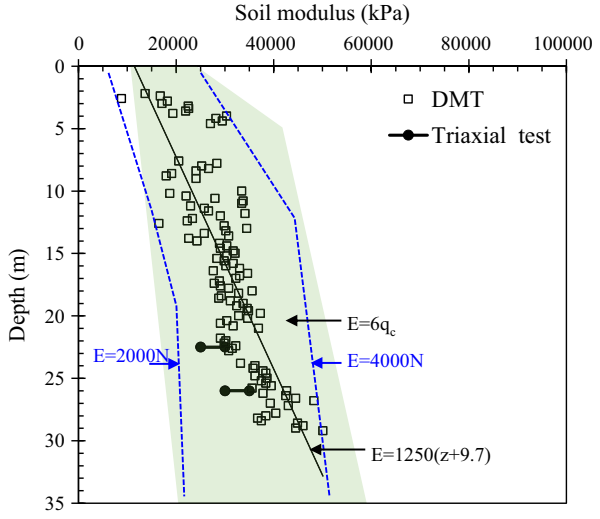

Fig. 12. Comparisons of sand moduli measured from the DMT and triaxial tests and those estimated by various empirical approaches.

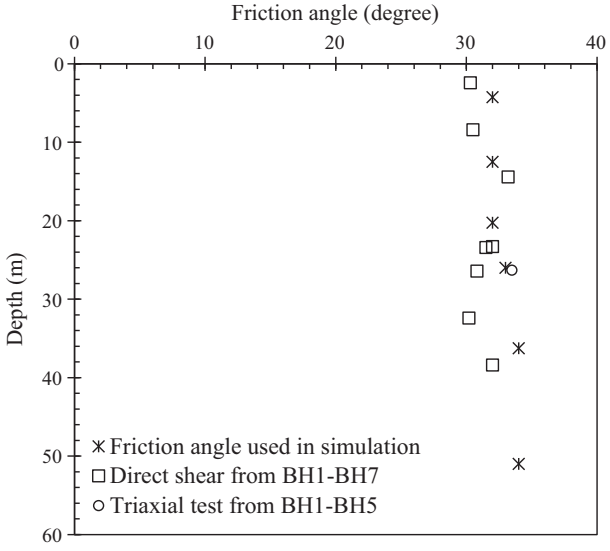

Fig. 13. Tested friction angles of sand from the site.

discussed to determine the soil parameters (Fig. 12). The DMT results show that the E values increase with depth from 10,000 to 33,000 kPa from the surface to the final excavation level. Fig. 12 shows a linear regression line, $E = 1250(z + 9.7)$ that is obtained from the DMTs. Although the soil modulus in the MC model is stress-independent (i.e., not a function of the stress state), the use of the E value estimated from the linear regression line in the MC model effectively takes into account the stress-dependent effect of E (i.e., E increases with depth) in the numerical simulation.

In addition to E measured from the DMTs, E is also estimated from the CPT results based on the correlation suggested by Kulhawy and Mayne [24]. Based on the theory of elasticity, E is determined as:

$$E = \frac{M(1+\nu)(1-2\nu)}{1-\nu} \tag{3}$$

where M is the constrained modulus, ν is the Poisson's ratio, and M is expressed as:

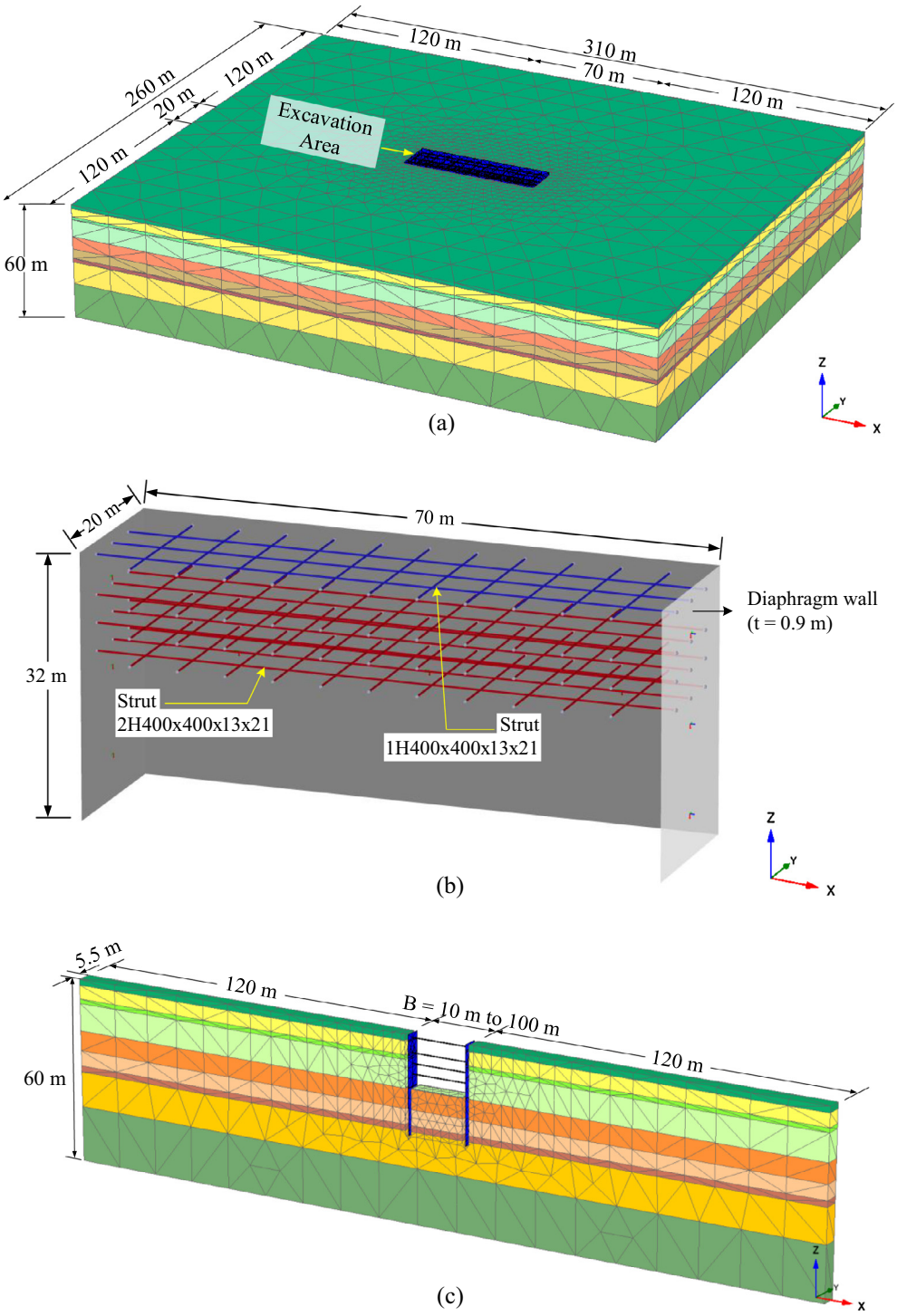

Fig. 14. Finite element model: (a) 3D benchmark model; (b) details of structural elements; (c) 3D plane strain model for the reference for the calculation of the PSR.

$$M = \alpha q_c \tag{4}$$

where α is a dimensionless coefficient that is closely related to the soil's relative density, which typically ranges from 3 to 8 for normally consolidated sand, and q_c is the tip resistance of the CPT. Considering the low N value as well as the high void ratio of the loose sand at the site, $\alpha = 8$ and $\nu = 0.3$ are input into Eqs. (3) and (4), so E is calculated as:

$$E = 6q_c \tag{5}$$

The values of E interpreted from the CPT results are plotted in Fig. 12 and are consistent with the values obtained from the DMT measurements.

The value of E is also estimated using SPT correlations. Based on a series of back analyses of monitoring data, Hsiung [7] suggested a correlation between E and SPT-N as follows:

$$E = 2000\ N(\text{kPa}) \tag{6}$$

Table 2
Input parameters of the MC model for sand layers using the effective stress and a drained analysis.

Layer	Depth (m)	Soil type	γ (kN/m^3)	N average	ϕ' (°)	c' (kPa)	E' (kPa)	ν'	ψ (°)
2	2.0–6.5	SM	20.9	8	32	0.5	21,500	0.3	2
4	8.0–17.0	SM	20.6	11	32	0.5	27,753	0.3	2
5	17.0–23.5	SM	18.6	11	32	0.5	37,440	0.3	2
6	23.5–28.5	SM	19.6	11	33	0.5	44,628	0.3	3
8	30.5–42.0	SM	19.6	22	34	0.5	57,449	0.3	4
9	42.0–60.0	SM	19.9	35	34	0.5	75,878	0.3	4

Table 3
Input parameters of the MC model for clay layers using the total stress and an undrained analysis.

Layer	Depth (m)	Soil type	γ (kN/m^3)	S_u (kPa)	E_u (kPa)	ν_u
1	0.0–2.0	CL	19.3	28	14,000	0.495
3	6.5–8.0	CL	19.7	21	10,500	0.495
7	28.0–30.5	CL	18.6	84	42,000	0.495

Stroud [19] presented a relationship between E and N values by collecting data from different soils, and he suggested that E decreases as the soil strain increases. Within the proper strain range of a retaining wall (~0.1%), Yong [25] suggested that E can be estimated as:

$$E = 4000\ N\ (\text{kPa}) \tag{7}$$

In addition, the Architectural Institute of Japan [18] recommended using $E = 2800\ N$ (unit in kPa), which is also commonly adopted for engineering practice. Fig. 12 shows the E values estimated from 2000 N to 4000 N. The E values estimated by the SPT correlations match the E values obtained from the CPT correlations and the DMT measurements.

Additionally, Fig. 12 shows two secant E values at strains of 0.1–0.3% (typical range of strains in deep excavations) interpreted from the triaxial stress-strain curves of sand specimens that were sampled from depths of 24 and 26 m. The secant E values range from 27,500 to 30,000 kPa, which are at the lower bound of the E values measured from the DMTs (Fig. 12). The lower values of E are thought to be caused by sample disturbance.

Finally, the E values based on linear regression from the DMT tests are used as an input for the subsequent FE analysis. The E values estimated by 2000 N and 4000 N are also selected for the FE analysis for comparison. As shown in Fig. 12, the E values that were directly measured from the shallow DMTs tend to be higher than those interpreted from linear regression because of the influence of stiff compacted backfill or the existence of old building foundations. As a result, an average value of E from the DMTs in the 1st layer of sand was taken as an input instead of that from the linear regression.

Several sets of direct shear tests were conducted during the site investigation phase to define the friction angle of the sand. The friction angle adopted in the analysis was thus taken from direct shear tests of soil samples that were collected from the construction site. Fig. 13 shows the friction angles of the sand, which range from 32 to 34 degrees and agree well with the direct shear and triaxial test results from nearby boreholes. This further confirms the reliability of the friction angle values used in the FE analyses.

Table 4
Input parameters for the diaphragm wall.

Parameter	Name	Value	Unit
Compressive strength of concrete	f'_c	28	MPa
Thickness	d	0.9	m
Young's modulus	E	24.8×10^6	kPa
Young's modulus × 70%	70%E	17.36×10^6	kPa
Unit weight	w	5.5	kN/m^3
Poisson's ratio	ν	0.2	

4. Finite element analyses

4.1. Soil model and input properties

A three-dimensional FE analysis, called a "benchmark analysis", was conducted to simulate the excavation in this study. The commercial software PLAXIS 3D, version 2013, was used as a numerical tool for the 3D analyses. Fig. 14 shows the 3D FE model of the benchmark analysis. The FE model consists of 50,364 ten-node tetrahedral elements with a total of 76,588 nodes. The dimensions of the FE model are 310 m × 260 m × 60 m. The base of the model was placed at the top of the mudstone layer, which is at a depth of 60 m below the ground surface. The distance from the lateral boundaries of the model to the retaining wall was 120 m, which is approximately seven times the excavation depth; this was suggested by Khoiri and Ou [11] for numerical modelling of deep excavations. Standard fixed conditions were applied to the FE model; horizontal movement was restrained on the lateral boundaries, and both horizontal and vertical movements were restrained on the bottom boundary of the model. Details of the structural elements (i.e., struts and diaphragm walls) and a 3D plane strain model for reference in the calculation of the PSR are also shown in Fig. 14b and c, respectively.

This study focuses on the 3D effects of the excavation on the wall deformation and the PSR value interpreted from the maximum lateral wall displacement. According to previous studies by Powire et al. [21], Ou [4], Kung et al. [5], Schweiger [8] and Khoiri and Ou [11], the constitutive soil model that is adopted in the numerical analysis has only a minor influence on the predicted wall displacements. Furthermore, limited information about some input soil properties and the considerably high computational cost limit the application of advanced constitutive soil models in 3D

Table 5
Input parameters for steel struts.

Strut level	Strut level	Preload (kN)	Section area (m^2)	EA (kN)	60%EA (kN)
Level 1	1H400 × 400 × 13 × 21	450	0.0219	4.59×10^6	2.75×10^6
Level 2	2H400 × 400 × 13 × 21	1000	0.0437	9.18×10^6	5.50×10^6
Level 3	2H400 × 400 × 13 × 21	1400	0.0437	9.18×10^6	5.50×10^6
Level 4	2H400 × 400 × 13 × 21	1400	0.0437	9.18×10^6	5.50×10^6

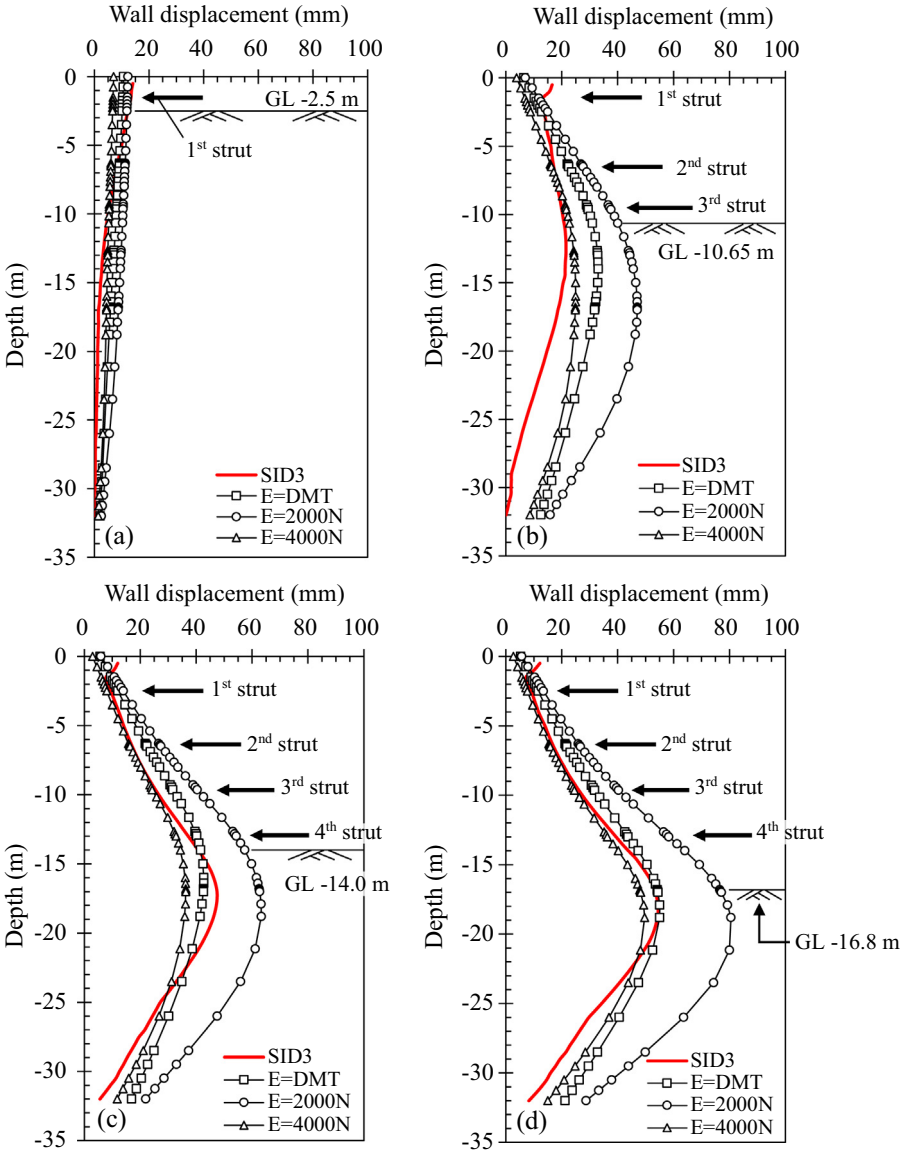

Fig. 15. Comparison of predicted and measured wall displacements on the long side at various excavation stages: (a) 1st stage; (b) 3rd stage; (c) 4th stage; (d) final excavation stage.

analyses. As a result, the linear elastic-perfectly plastic MC model was selected as the soil model in the benchmark analysis. This study aims to assess the applicability and suitability of FE analyses that use a simple and rational MC model with parameters that can be easily obtained from in-situ or laboratory tests to predict the wall deformation induced by an excavation.

Tables 2 and 3 summarize the input parameters of the MC model for the sand and clay layers. The sand layers were analysed using an effective stress analysis under drained conditions, and the clay layers were analysed using a total stress analysis under undrained conditions. The selections of two key soil parameters, E and ϕ, have been described in detail previously. A low cohesion value, $c' = 0.5$ kPa, was assigned to the sand layers to avoid numerical instability and problems with the calculations in PLAXIS. The drained Poisson's ratio was taken to be $\nu' = 0.3$ as suggested by PLAXIS 3D [26] and Khoiri and Ou [11]. For sands with $\phi' > 30°$, the soil dilation angle ψ is estimated as:

$$\psi = \phi' - 30° \tag{8}$$

The initial soil stress conditions were generated assuming that the state of soil stress is under at-rest conditions, which can be determined by the at-rest earth pressure coefficient proposed by Jaky [27]:

$$K_o = 1 - \sin\phi' \tag{9}$$

For the undrained analysis of the total stress of the clay layers, the undrained friction angle $\phi_u = 0$, undrained shear strength S_u, undrained Young's modulus E_u, undrained Poisson's ratio $\nu_u = 0.495$, and undrained dilation angle $\psi_u = 0$ were input into the MC model. The values of S_u were taken from the triaxial unconsolidated-undrained test results. An undrained Poisson's ratio $\nu_u = 0.495$ (≈ 0.5) was adopted to simulate the incompressible behaviour of saturated clay under undrained conditions. According to Bowles [28], Lim et al. [29], Likitlersuang et al. [10], and Khoiri and Ou [11], the E_u value can be computed using the following empirical equation:

$$E_u = 500 S_u \tag{10}$$

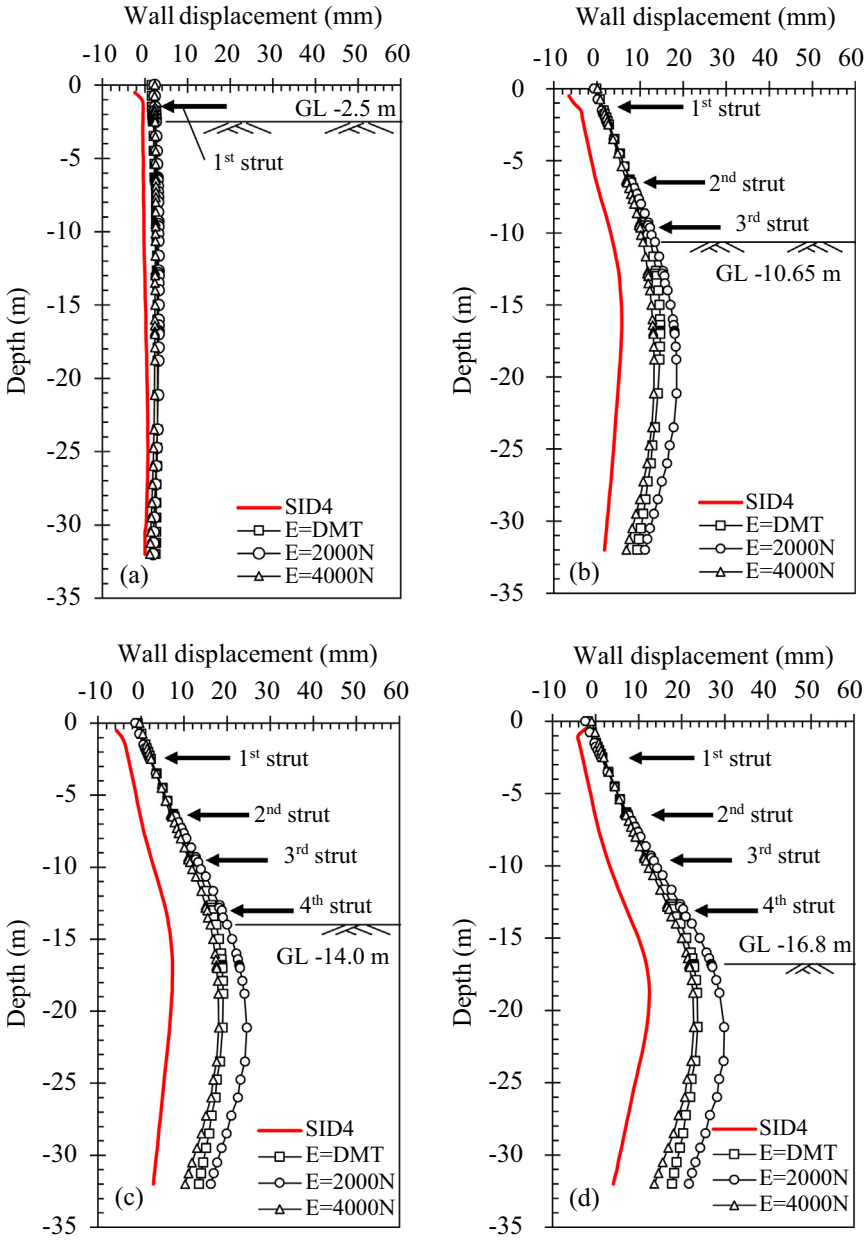

Fig. 16. Comparison of predicted and measured wall displacements on the short side at various excavation stages: (a) 1st stage; (b) 3rd stage; (c) 4th stage; (d) final excavation stage.

Notably, the simulated clay layers have a minor influence on the wall behaviour because the clay layers at the site were very thin compared to the sand layers.

4.2. Structural model and input properties

Tables 4 and 5 list the input parameters of the diaphragm wall and steel struts used in the analysis. The diaphragm wall was simulated by plate elements, and the steel struts were modelled by node-to-node anchor elements. The behaviours of both the plate elements and the node-to-node anchor elements were governed by the linear-elastic model, which requires two input parameters: Young's modulus and Poisson's ratio. Poisson's ratio of the structural elements was taken to be 0.2 for both the diaphragm wall and the steel struts. The Young's modulus of the diaphragm wall was calculated by the formula of ACI Committee 318 [30] as follows:

$$E = 4700\sqrt{f'_c} \quad \text{(MPa)} \tag{11}$$

where f'_c (MPa) is the standard compressive strength of the concrete. The Young's modulus of the steel struts was assigned to be 2.1×10^5 (MPa). As suggested by Ou [4], the stiffnesses of the diaphragm wall and steel struts were reduced by 30% and 40% from their nominal values, respectively, to consider defects and cracks in the diaphragm wall caused by the bending moments and to account for the stiffness reduction of the steel struts due to repeated use and improper installation. The unit weight of the plate was subtracted from the unit weight of the soil because the wall was modelled as non-volume elements. The interface elements were also included in the simulation to represent the interaction between the soil and the diaphragm wall. As suggested by Khoiri and Ou [11] and the default value suggested by PLAXIS 3D [26], the interface reduction parameter between the wall and the soil is assumed as $R_{inter} = 0.67$.

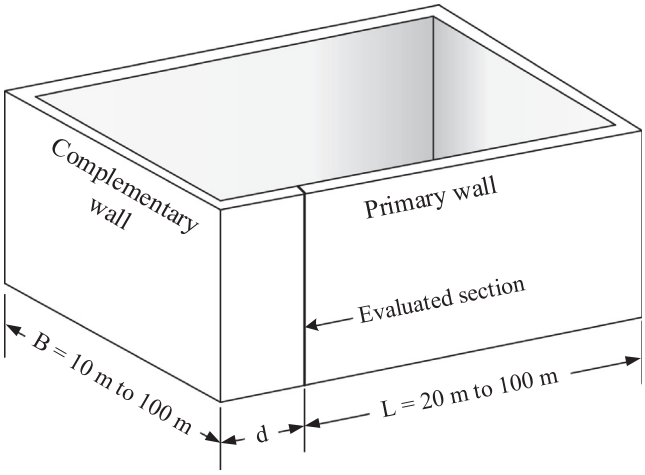

Fig. 17. Definitions of the excavation length *L*, excavation width *B* and distance from the evaluated section to the excavation corner *d*.

5. Results and discussion

5.1. Comparison between measured and predicted results

The wall displacements induced by the excavation are examined and discussed in this section. Fig. 15 compares the predicted and measured wall displacements on the long side at various stages of excavation. The measured wall displacement was taken from the inclinometer reading of SID3, which was installed at the centre of the long diaphragm wall. The predicted maximum lateral wall displacements using *E* from the DMTs increase from 10 mm in the 1st excavation stage to 54 mm in the final excavation stage. The comparison shows that the predictions using *E* from the DMTs slightly overestimate the wall displacement in the 1st and 3rd excavation stages but agree well with the measured displacements in the 4th and final excavation stages. The predictions using $E = 2000\ N$ overpredict the wall displacements at all excavation stages because the lower bound value of the SPT-*N* correlation was used to estimate the soil modulus in the simulation. Overall, the predicted results using *E* from the DMT and SPT-*N* correlations appear to accurately predict the depth with the maximum lateral wall displacement. Thus, the use of the MC model with the soil modulus obtained from the DMTs yields reasonable predictions of the excavation-induced wall displacements in loose to medium dense sands.

The wall displacement on the short side was also examined. The inclinometer located at the centre of the wall on the short side, SID4, was selected for comparison. Fig. 16 compares the predicted and measured wall displacements on the short side at various excavation stages. The observations show that the wall movement gradually increases from no movement in the 1st excavation stage to 12 mm at the end of excavation. The maximum displacement corresponds to the depth of the final excavation level. All of the predictions indicated displacements of approximately 3 mm in the 1st excavation stage and then range from 24 to 33 mm in the final excavation stage, which is almost twice as large as the observed values. The discrepancy between the measured and predicted wall displacements is likely attributed to the heavy corner diagonal bracing of each strut, which is shown in the strut layout in Fig. 2. The heavy corner diagonal bracing, which is not considered in the numerical simulation, likely stiffened the wall system and reduced the wall displacement on the short side. Several references [31,32] indicated that wall deformations are connected with small strain properties of soil as well as relative stiffness of soil and

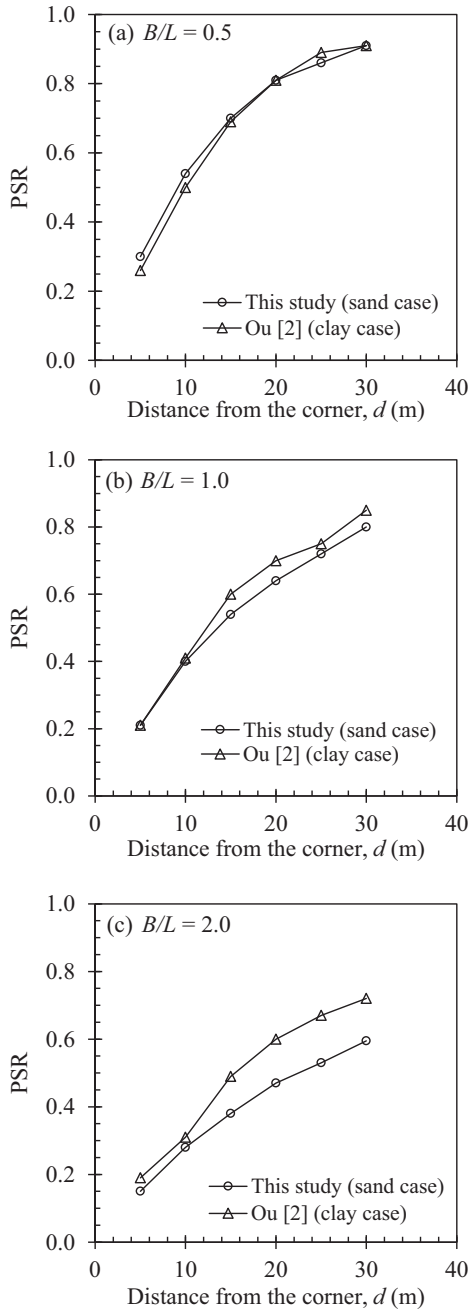

Fig. 18. Variation of PSR with *d* for various *B*/*L* values: (a) *B*/*L* = 0.5; (b) *B*/*L* = 1.0; (c) *B*/*L* = 2.0.

retaining and strutting system. It is seen that the displacement on the short side is much smaller than that on the long side so soil stiffness on the short side should be much higher. Further investigation is required to include the effect of factors stated above in the numerical analysis.

Fig. 6 compares the measured and predicted strut loads at the 2nd level strut during the entire excavation period. The comparison reveals that the measured and predicted strut loads agree fairly well in both the magnitude and the overall trend with time. Because the predicted strut load from the FE analysis is a function of the strut deformation, which is related to the wall deformation, the good agreement between the predicted and measured wall displacements in Fig. 15 ensures good results in predicting the strut loads. This comparison again confirms the applicability and suit-

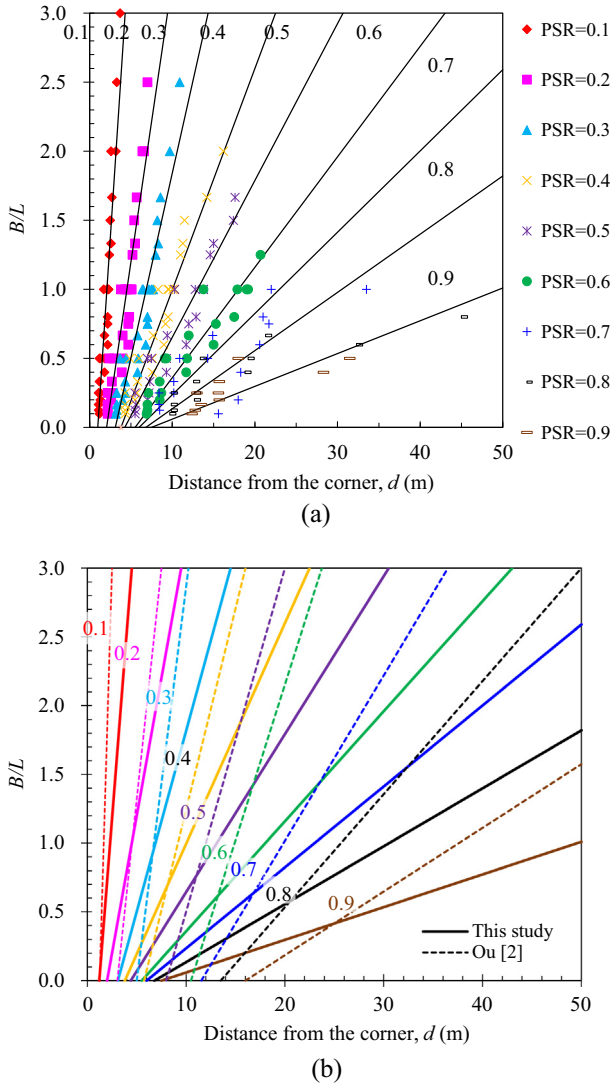

Fig. 19. PSR charts: (a) excavations in loose to medium dense sands; (b) comparison of PSR values in clay and in sand.

ability of 3D FE models for predicting the wall behaviour due to excavations in sand.

5.2. 3D effect of excavation and plan strain ratio

After the numerical model was verified, a series of parametric studies was performed by varying the excavation length and width to evaluate the 3D effects of the excavation on the wall displacement. Fig. 17 shows the definitions of the excavation length L, excavation width B and distance from the evaluated section to the excavation corner d. In the parametric study, the input parameters for the soils and structures remained unchanged. Only the dimensions of the excavation (i.e., L and B) were varied; the values of L are 20, 40, 60, 80 and 100 m, and the values of B are 10, 20, 40, 60, 80 and 100 m. A total of 30 3D simulations were conducted in the parametric study. In addition, a 3D plane strain model was developed (Fig. 14c), in which the thickness of the model was equal to the horizontal spacing of the steel struts; i.e., 5.5 m. The 3D plane strain model was used to mimic a 2D model, which is commonly used in practical design, and the wall displacement of the 3D plane strain model served as the reference value for the wall displacement under plane strain conditions.

The 3D effect on the wall displacement is quantitatively assessed using the PSR, which is the ratio of the maximum wall deflection of a section of the wall to the maximum wall deflection of the section under plane strain conditions. This ratio was first proposed by Ou et al. [2] as follows:

$$PSR = \frac{\delta_{hm,d}}{\delta_{hm,ps}} \tag{12}$$

where $\delta_{hm,d}$ is the maximum wall deflection at a certain section along the wall, and $\delta_{hm,ps}$ is the maximum wall deflection of the section under plane strain conditions.

Fig. 18 shows the PSR results for $B/L = 0.5$, 1.0, and 2.0. For all three cases, the PSR increases gradually with increasing d and then reaches a constant value at large d, which indicates that the corner effect disappears as the distance from the section to the corner increases. In addition, the PSR appears to be increase rapidly as B/L decreases. Fig. 19a shows the relationship between B/L and d for various PSR values. At a given d, B/L would have a significant impact on the PSR. The displacements easily reach plane strain conditions with very narrow excavations (smaller B/L) but not with wide ones. The influence of the corner effect decreases when d is greater than 30 m; the PSR value exceeds 0.6 regardless of the B/L. Under these conditions, the maximum wall displacement at a certain d is not significantly smaller than the maximum displacement under plane strain conditions, which suggests the decreasing influence of the 3D effect on the wall displacement. The proposed PSR chart (Fig. 18a) provides an alternative to transfer wall displacements from a 2D analysis to one that considers the 3D effect, which therefore allows a practical design (typically in 2D) to account for the 3D effects of an excavation on wall deformation.

Figs. 18 and 19b compare the PSR values in sand that were calculated in this study and those calculated in clay by Ou et al. [2]. The comparisons show that the proposed PSR values in this study are different from that in previous studies of deep excavations in clay, especially for cases when d and B/L are large. As shown in Fig. 18c, the PSR values in this study are substantially lower than those in clay by Ou [2] for $B/L = 2.0$ and $d > 10$ m. Because the same construction method (i.e., bottom-up method) was adopted for the background cases that were used to determine the PSR values in both studies, the different subsurface soil conditions (sand and clay) and analysis types (drained and undrained) led to the discrepancies in the PSR charts. As described above, soil stiffness might be higher on the short side so B/L ratio might also be correlated to soil modulus and PSR values. Based on the comparison results, this study demonstrated that the soil and analysis types have significant effects on the wall behaviour of deep excavations.

6. Conclusions

This paper presents a study that evaluates the 3D effects of a deep excavation in loose to medium dense sands on wall displacements. An FE analysis was conducted to model a deep excavation in Kaohsiung, Taiwan, to verify the performance of a 3D FE model in predicting wall displacements. Thereafter, a series of parametric studies was performed by varying the excavation length and width to determine the PSR and establish its relationships with the excavation aspect ratio B/L and the distance from the evaluated section to the excavation corner d. The following conclusions were drawn from the results of this study:

1. For an excavation in sand, the wall initially behaves in cantilever-mode and then changes to prop-mode after the struts are installed. The 3D corner effect exists because the wall

displacements measured by the inclinometer located on the long side of the diaphragm wall are considerably greater than those on the short side.

2. The distributed prop load (DPL) suggested by Twine and Roscoe [16] and the apparent earth pressure diagram for sand suggested by Peck [17] generally agree well with the DPL calculated in this study at depths from 3 to 9 m. The two empirical equations, which include the increase of water pressure with depth in the calculation, overestimate the measured DPLs at depths below 9 m.
3. The soil modulus E plays a key role in predicting the wall displacement induced by an excavation. The MC model with the soil modulus obtained from in-situ DMT measurements can give reasonable predictions for wall displacements induced by deep excavations in loose to medium dense sand. The predictions using $E = 2000\ N$ overpredicted the wall displacements in all excavation stages because the lower bound value of the SPT-N correlation was used for the soil modulus in the simulation.
4. The observed wall displacements on the short side of the diaphragm wall tend to be smaller than the predicted values because the heavy corner diagonal bracing of each strut stiffened the wall system and reduced the wall displacements. Further investigation is needed to include the effect of corner diagonal bracing of struts in the numerical analysis.
5. A relationship between B/L and d for various PSR values is established to quantitatively assess the 3D effects on the wall displacements. With a combination of large d (large distance from the corner) and small B/L (narrow excavation aspect ratio), the displacements easily reach plane strain conditions, which suggests the decreasing influence of the 3D effect on the wall displacements.
6. The comparison results revealed that the proposed PSR in this study is different from those in previous studies of deep excavations in clay, especially for cases when d and B/L are large. The different subsurface soil conditions (sand and clay) and analysis types (drained and undrained) led to the discrepancies between the PSR charts. Based on the comparison results, this study demonstrated that the soil and analysis types have a significant effect on the wall behaviour of deep excavations.

Finally, for engineering practice, the proposed PSR chart provides an alternative for transferring the wall displacement from a 2D analysis to one that considers the 3D effects, which therefore can provide designers with a practical reference to account for the 3D effects of excavations on wall deformations.

Acknowledgements

The authors would like to thank the Ministry of Science and Technology, Taiwan, for financial support for this project (Research Grant Number 100-2622-E-151-021-CC3). In addition, assistance from Mr. Juei-Jen Chang and Resources Engineering Services Inc. for the field work and testing is appreciated. Finally, help with the numerical analyses by Dr. Dao, Sy Dan, former PhD student at the National Kaohsiung University of Applied Sciences, is appreciated.

References

[1] Clough GW, O'Rourke TD. Construction-induced movements of in situ walls. In: Design and performance of earth retaining structures. Geotech spec publ 25. ASCE; 1990. p. 439–70.
[2] Ou CY, Chiou D, Wu T. Three-dimensional finite element analysis of deep excavations. J Geotech Eng 1996;122:337–45. http://dx.doi.org/10.1061/(ASCE)0733-9410(1996) 122:5(337).
[3] Ou CY, Shiau B, Wang I. Three-dimensional deformation behavior of the Taipei national enterprise center (TNEC) excavation case history. Can Geotech J 2000;37:438–48. http://dx.doi.org/10.1139/t00-018.
[4] Ou CY. Deep excavation: theory and practice. Netherlands: Taylor & Francis; 2006.
[5] Kung GT, Juang CH, Hsiao EC, Hashash YM. Simplified model for wall deflection and ground-surface settlement caused by braced excavation in clays. J Geotech Geoenviron Eng 2007;133:731–47. http://dx.doi.org/10.1061/(ASCE)1090-0241(2007) 133:6(731).
[6] Lin DG, Woo SM. Three-dimensional analyses of deep excavation in Taipei 101 construction project. J Geoeng 2007;2:29–41.
[7] Hsiung BCB. A case study on the behaviour of a deep excavation in sand. Comput Geotech 2009;36:665–75. http://dx.doi.org/10.1016/j.compgeo.2008.10.003.
[8] Schweiger HF. Influence of constitutive model and EC7 design approach in FEM analysis of deep excavations. In: Proceedings of ISSMGE international seminar on deep excavations and retaining structures, Budapest, Hungary. p. 99–114.
[9] Wang JH, Xu ZH, Wang WD. Wall and ground movements due to deep excavations in Shanghai soft soils. J Geotech Geoenviron Eng 2010;136:985–94. http://dx.doi.org/10.1061/(ASCE)GT.1943-5606.0000299.
[10] Likitlersuang S, Surarak C, Wanatowski D, Oh E, Balasubramaniam A. Finite element analysis of a deep excavation: a case study from the Bangkok MRT. Soils Found 2013;53:756–73. http://dx.doi.org/10.1016/j.sandf.2013.08.013.
[11] Khoiri M, Ou C. Evaluation of deformation parameter for deep excavation in sand through case histories. Comput Geotech 2013;47:57–67. http://dx.doi.org/10.1016/j.compgeo.2012.06.009.
[12] Finno RJ, Arboleda-Monsalve LG, Sarabia F. Observed performance of the One Museum park west excavation. J Geotech Geoenviron Eng 2015;141:04014078. http://dx.doi.org/10.1061/(ASCE)GT.1943-5606.0001187.
[13] Orazalin Z, Whittle AJ, Olsen MB. Three-dimension analysis of excavation support system for the Stata Centre Basement on the MIT campus. J Geotech Geoenviron Eng 2015;141:0501500.
[14] Hsieh PG, Ou CY, Lin YK, Lu FC. Lessons learned in design of an excavation with the installation of buttress walls. J Geo Eng 2015;10:67–73.
[15] Nikolinakou MA, Whittle AJ, Savidis S, Schran U. Prediction and interpretation of the performance of a deep excavation in Berlin sand. J Geotech Geoenviron Eng 2011;137:1047–61. http://dx.doi.org/10.1061/(ASCE)GT.1943-5606.0000518.
[16] Twine D, Roscoe H. Temporary propping of deep excavations-guidance on design, Ciria C517. London: Construction Industry Research and Information Association; 1999.
[17] Peck RB. Deep excavation and tunneling in soft ground. In: Proceedings of the 7th international conference on soil mechanics and foundation engineering, Mexico City, Mexico. p. 225–90.
[18] Architectural Institute of Japan. Recommendations of design of building foundation. Japan. (Interface [Japanese] 2001).
[19] Stroud MA. The standard penetration test- its application and interpretation. London: Thomas Telford; 1989. p. 29–49.
[20] Skempton AW. Standard penetration test procedures and the effects in sands of overburden pressure, relative density, particle size, ageing and overconsolidation. Geotechnique 1986;36:425–47. http://dx.doi.org/10.1680/geot.1986.36.3.425.
[21] Powrie W, Chandler RJ, Carder DR, Watson GVR. Back-analysis of an embedded retaining wall with a stabilizing base slab. Proc Inst Civ Eng Geotech Eng 1999;137:75–86.
[22] Jardine RJ, Potts DM, Fourie AB, Burland JB. Studies of the influence of non-linear stress–strain characteristics in soil–structure interaction. Geotechnique 1986;36:377–96. http://dx.doi.org/10.1680/geot.1986.36.3.377.
[23] Burland J, Kalra J. Queen Elizabeth Ii conference centre: geotechnical aspects. Proc Inst Civ Eng 1986;80:1479–503. http://dx.doi.org/10.1680/iicep.1986.527.
[24] Kulhawy FH, Mayne PW. Manual on estimating soil properties for foundation design. Elctric Power Research Institute; 1990. p. 1493–6. EL-6800, Research Project.
[25] Yong KY. Learning lessons from the construction of Singapore Downtown line (DTL). In: Proceedings of international conference and exhibition on tunneling and underground space, Kuala Lumpur, Malaysia.
[26] PLAXIS. Reference manual. Amsterdam, The Netherlands: Plaxis BV; 2013.
[27] Jaky J. The coefficient of earth pressure at rest. J Soc Hung Archit Eng 1944;7:355–8 [in Hungarian].
[28] Bowles JE. Foundation analysis and design. 5th ed. New York: McGraw Hill; 2009.
[29] Lim A, Ou CY, Hsieh PG. Evaluation of clay constitutive models for analysis of deep excavation under undrained conditions. J Geo Eng 2010;5:9–20.
[30] ACI. Committe 318: building codes requirements for reinforcement concrete; 1995.
[31] Ng CWW, Yan WM. A true three- dimensional numerical analysis of diaphragm walling. Geotechnique 1999;49(6):825–34.
[32] Tang YG, Kung GTC. Investigating the effect of soil models on deformations caused by braced excavation through an inverse- analysis technique. Comput Geotech 2010;37:769–80.